Computational analysis of conjugate heat transfer in a 2D rectangular channel with mounted obstacles using lattice Boltzmann method

Majid Nejadseifi*. Shervin Karimkashi. Tero Tynjälä*. Payman Jalali***

**Laboratory of Thermodynamics, School of Energy Systems, Lappeenranta-Lahti University of Technology, Lappeenranta, 53850, Finland (Tel: 358-415750813; e-mail: majid.nejadseifi@lut.fi, tero.tynjala@lut.fi, payman.jalali@lut.fi).*

*** Laboratory of Energy conversion and systems, Department of Mechanical Engineering, School of Engineering Sciences, Aalto university, Espoo, 02150, Finland (Tel: +358505602614; e-mail: shervin.karimkashiarani@aalto.fi)*

Abstract: The objective of this paper is to investigate the fluid flow and conjugate heat transfer in a 2D channel using lattice Boltzmann method (LBM). In this work, fluid flow and heat transfer are studied for the Reynolds numbers varying between 250 and 1000. The working fluid in the simulations is air with the Prandtl number of 0.72. At the Reynolds number of 600, the effect of different conductivity ratio (1, 10, 100, 400) between solid and fluid are investigated. Furthermore, at this Reynolds number, the distance between obstacles for the conductivity ratio of 10 is evaluated. The results show that any increase in Reynolds number leads to a heat transfer improvement. Moreover, increase in the conductivity ratio leads to an isothermal surface and enhanced heat transfer. The more the distance between the obstacles, the better the heat transfer rate. The results obtained from LBM are in good agreement with experimental and conventional computational fluid dynamics methods.

Keywords: Lattice Boltzmann Method (LBM), Conjugate heat transfer, Nusselt number, Prandtl number

1. INTRODUCTION

In recent years, the computer technology and e-commerce have significantly progressed. Over time, electronic components have become more compact and occupy smaller space. As the components are more compact, the processing speed has increased considerably. Due to the smaller space occupied by the components, temperature resistance is increased against heat transfer and the performance has dropped with increasing temperatures in electronic equipment.

In electronic cooling, forced convection is often the dominant heat transfer mode, with the cooling agent being either a common gas or a heat-transferring liquid. Various techniques have been proposed to enhance the heat transfer rate between the solid electronic devices and the adjacent cooling fluid, and their thermal performance has been evaluated. Among these techniques, the use of solid fins Chen et al. (1997) and blocks Sara et al. (2001) have proven to be efficient. Additionally, Ramesh et al. (2021) has done an extensive review of various numerical and experimental studies that have investigated methods for enhancing heat transfer in cooling devices.

Chikh et al. (1998) conducted a numerical investigation on forced convection heat transfer within a partially heated channel, focusing on the impact of porous obstacles installed on the heated section to enhance the heat transfer rate. Their results demonstrated that using porous obstacles under certain flow and thermal conditions lead to a 90% drop in wall temperature.

There have been many studies on the heat transfer of the extended surfaces in channels. Bhowmik et al. (2009) examined pressure loss and heat transfer in a channel with two bending blades, and provided connections for a laminar, transient and turbulent flow in a marginal geometry. Improvement of heat transfer for equally spaced plates was done experimentally by Leung et al. (1999). They examined the parameters including the diameter of the slopes, the geometry and height of the cavities, and the Reynolds number. They concluded that for the ducts, heat transfer decreases with increasing the diameter of the duct due to the decrease of the surface. The effect of cubic layout on turbulent flow was experimentally investigated by Meinders et al. (2002). They concluded that, with increasing flow velocity, fluid flow would be affected by the distance between extended surfaces. Nazari et al. (2013) investigated a heat transfer problem in a closed compartment with a vertical or horizontal porous layer using LBM.

Numerical simulations that use conventional computational fluid dynamic (CFD) techniques, such as finite volume and finite difference methods, are difficult to apply in complex boundary conditions, for instance in heat transfer problems at the interface between the fluid and solid instead of a constant temperature or heat flux condition. Using such a conjugate boundary condition in CFD methods will increase the computational cost. Therefore, it is required to use a less expensive method. One of the most useful methods for this kind of problems is the Lattice Boltzmann Method (LBM).

LBM is a reliable approach for studying numerous fluid and heat transfer issues, including multi-component and multiphase flows, microflows, turbulent flows, fluid-solid interactions, and both forced and natural convection in

complex geometries. Based on the kinetic theory of gases with a mesoscopic approach, LBM is widely used due to its effectiveness in handling physical problems with intricate geometries and boundary conditions. Consequently, it is frequently employed for solving fluid flow problems in porous media. Ataei-Dadavi et al. (2019) studied fluid flow and heat transfer in a porous cavity with side heating. Results showed that heat transfer decreased with porous media compared to a non-porous cavity. They developed a new method to predict Nusselt numbers for such cavities. Nejadseifi et al. (2024) used the lattice Boltzmann method to computationally study porous media composed of monodisperse square obstacles within the Darcy regime. Mirahsani et al. (2023) investigated heat transfer enhancement in a partially heated channel with porous obstacles. Using a lattice Boltzmann method, the flow and temperature fields were analyzed. Optimal design parameters, including the height, pitch, and permeability of the porous blocks, were determined. Results showed that the optimal block height and pitch depend on the Darcy number (Da). The impact of obstacle geometry and porous material distribution on thermal performance was also examined. Matsuda et al. (2024) enhanced enthalpic lattice Boltzmann method (LBM) to simulate conjugate heat transfer in non-homogeneous media with time-dependent thermal properties. Their findings highlighted the potential of the modified LBM for simulating complex heat transfer in a non-homogeneous media and in optimizing heat exchanger designs. Paknahad et al. (2023) investigated pore-scale flow and conjugate heat transfer in high-porosity open-cell metal foams. They showed that lower porosity foams transition from the Darcy to non-Darcy flow regime at lower Reynolds numbers, while pore density has minimal impact on this transition. Heat transfer results indicated that metal foams cool rapidly at high flow velocities, with minimal temperature rise in the fluid.

Although LBM has been successfully applied to simulating fluid flows in small-scale channels, there are few reports of using LBM to simulate fluid-solid coupling heat transfer in such channels. In this study, the fluid flow and heat transfer within the channel with extended surfaces is investigated and lattice Boltzmann equations are used for simulations. The simulation setup is a channel with insulated internal surfaces, wherein heat transfer occurs through extended surfaces; In this setup, effects of changing parameters such as Reynolds number, conduction coefficient ratio and obstacles distance are investigated. It is assumed that there is a constant heat flux at the bottom of the obstacles. Validation of the results shows a good agreement with other works.

2. METHODOLOGY

2.1 Lattice Boltzmann Method

In recent years, LBM has been developed as a powerful simulation method to simulate many fluid mechanic problems. This method, based on the kinetics of gases theory, has been considered as a powerful numerical technique for simulating fluid flow and heat transfer (Paknahad et al., 2023, Ramesh et al., 2021) Compared to the conventional CFD methods, this method has several advantages. The conventional CFD methods discretize mass, momentum, and energy equations, and solve them based on macroscopic quantities such as velocity and pressure. Unlike CFD, LBM uses the number of finite speeds created on a regular lattice to solve problems (Noble et al., 1996).

2.2 Mathematical description of fluid flow and heat Transport Equations:

In contrast with the conventional macroscopic Navier–Stokes approach, the lattice Boltzmann method utilizes a mesoscopic simulation model to represent fluid flow (Suss et al., 2023). This technique is based on modeling the movement of fluid particles in different directions to derive macroscopic fluid characteristics, such as velocity and pressure. In this method, the fluid domain is divided into uniform cells, each containing a set number of Distribution Functions that represent fluid particles movement in specific discrete directions. Various LBM models are available depending on the dimensionality(2D-3D) and the number of velocity directions. This study focuses on two-dimensional 2D flow using a 2D square lattice with nine velocities, known as the D2Q9 model. The velocity vectors of the D2Q9 model are labeled as c0 to c8. The discrete velocities of the D2Q9 model are:

$$e_i = \begin{cases} (0,0) & i = 0 \\ (\pm 1,0)c, (0,\pm 1)c & i = 1,2,3,4 \\ (\pm 1,\pm 1)c & i = 5,6,7,8 \end{cases} \quad (1)$$

Under equilibrium conditions, macroscopic quantities can be measured before allowing the particles to move and collide in the next time step. In standard single relaxation time (SRT) lattice Boltzmann (LB) models, the BGK (Bhatnagar-Gross-Krook) model (Zou and He, 1997) is used to represent collisions, as described in Eq. (2). In this equation, f_i denotes the density distribution function in direction i, and e_i represents the discretization direction. Additionally, Δt is the LBM time step, and τ is the dimensionless relaxation time provided in Eq. (3).

$$f_i(x + e_i \Delta t, t + \Delta t) = f_i(x,t) - \frac{\Delta t}{\tau}[f_i(x,t) - f_i^{eq}(x,t)] \quad (2)$$

where:

$$\tau = 3\nu + \frac{1}{2} \quad (3)$$

where $c = \frac{\Delta x}{\Delta t}$ and i is an index for directions. The equilibrium distribution function $f_i^{eq}(x,t)$is calculated as (4):

$$f_i^{eq}(x,t) = \omega_i \rho \left(1 + \frac{u.e_i}{{c_s}^2} + \frac{(u.e_i)^2}{2{c_s}^4} - \frac{u^2}{2{c_s}^2}\right) \quad (4)$$

In the chosen D2Q9 model, the speed of sound c_s is equal to $\sqrt{3}$ in the specified value. Additionally, ω_i is the weight function represented by (5) as:

$$\rho = \sum_{i=0}^{8} f_i \quad , \quad V = \frac{1}{\rho}\sum_{i=0}^{8} f_i\, e_i \tag{5}$$

$$\omega_i = \begin{cases} 4/9 & i = 0 \\ 1/9 & i = 1,2,3,4 \\ 1/36 & i = 5,6,7,8 \end{cases} \tag{6}$$

In summary, the SRT-LBM process includes three main steps: (1) calculating the distribution function within the simulation domain, (2) computing collisions at each time step, and (3) streaming, or transferring the distribution function to neighboring nodes (Nejadseifi et al.,2024).

The distribution function for the thermal LBM can be represented as:

$$g_i(x + e_i\Delta t, t + \Delta t) = g_i(x,t) - \frac{\Delta t}{\tau}[g_i(x,t) - {g_i}^{eq}(x,t)] \tag{7}$$

The corresponding equilibrium distribution functions for fluid and solid are defined as follows (Mohammad, 2007):

$${g_i}^{eq}(x,t) = \omega_i T\left(1 + \frac{u.e_i}{{c_s}^2}\right) \tag{8}$$

$${g_i}^{eq}(x,t) = \omega_i T \tag{9}$$

Finally, for both solid and fluid, the temperature field is computed as:

$$T = \sum_{i=0} g_i \tag{10}$$

3. RESULTS AND DISCUSSION

The physical geometry used for calculations is shown in Fig. 1. The fluid flow is assumed laminar, incompressible, viscous, and Newtonian. The length of the entrance to the channel (Lin) before the obstacles is 6 times the obstacle's height. The length of the outer part of the channel, which is extended after the second obstacle (Lout), has been selected to be long enough for vortices observation. For this reason, the length of the outlet portion of the channel, which is located after the second obstacle, is 8H where H is the height of the channel.

The bounce back scheme is used for representing the wall boundary condition. In the bounce back scheme, it is assumed that the particles moving towards solid boundaries are returned into the fluid. Therefore, the distribution functions that are toward the wall bounced back in the opposite direction. The fully developed inlet velocity profile is set as $u_0(y) = 4u_{max}(Hy - y^2)/H^2$, and a negligible compressible flow is assumed (the maximum velocity is 0.1 in the input current). The unknown distribution functions in the input and output sections of the channel are obtained using the Zou and He. (1997) boundary function. The adiabatic boundary condition is employed on the walls. However, for the parts of the walls which include obstacles, non-zero temperature gradient and constant heat flux boundary conditions govern at the bottom part of the obstacle (q=1). On the boundaries between solid obstacles and fluid, the equilibrium distribution function, as well as the conductivity values for the fluid and solid, is changed. At the interface of the solid obstacles and fluid, the continuity of heat flux and temperature is naturally satisfied.

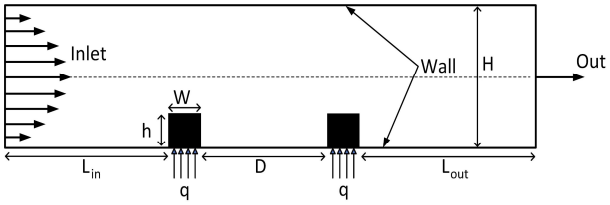

Fig 1. Schematic diagram of the problem geometry.

3.1 Grid independence test and code validation

The numerical simulations are carried out by a FORTRAN in-house code. To ensure the accuracy of the written code, a comparison is made between different studies to ensure a dimensionless reattachment study (Xr/L). These results are compared with the results of CFD(ANSYS-Fluent 2021 R2) software, (Korichi and Oufer, 2005; Pirouz et al., 2011). The fluid flow at the channel entrance has parabolic state and Reynolds number, which varies between 250 and 1000. Fig. 2 shows the dimensionless reattachment length for Reynolds numbers below 1000. The results show good agreement with other studies.

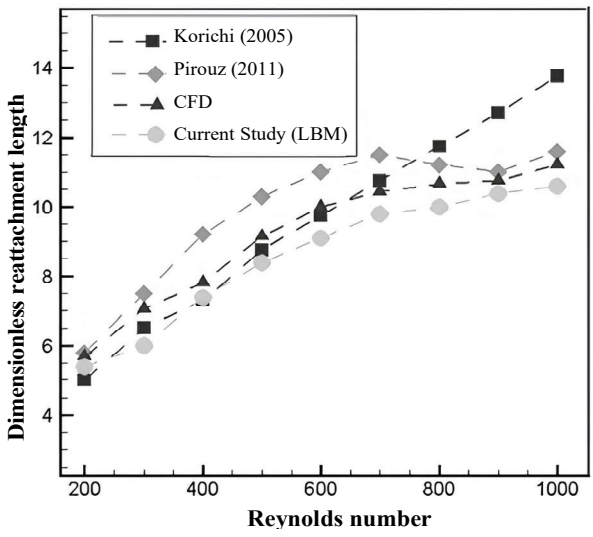

Fig. 2. Dimensionless reattachment length comparison for various Reynolds Number for a single obstacle.

The second validation is for grid independency. Validation is done for Reynolds numbers 500 and 750. The number of lattices required for code convergence is considered. (The channel width is 96, 128, and 160 lattice). The mean Nusselt number on the two obstacles for these lattices are compared with each other. Table 1 shows that for the range of Re that

have been studied, with 160 points across the channel, acceptable results are achieved. As Re increases, the lattice size needs to be finer: for example, when the Re reaches 500, the difference in the results for 96 lattice approaches 2% and this lattice is no longer suitable for such Re value, and that is why the number of grids needs to be higher (160 lattice).

Table 1. Effect of resolution on the mean Nusselt Number at different Reynolds numbers

Obstacle	Re	Mean Nusselt number		
		96 Grid	128 Grid	160 Grid
1	500	9.82 (1.44%)	9.91(0.6%)	9.97
2	500	8.08 (1.92%)	8.17(0.8%)	8.24
1	750	11.25 (1.83%)	11.33 (1.16%)	11.5
2	750	10.14 (2.42%)	10.23 (1.52%)	10.40

The third validation is associated with the thermal part of the written code. The flow inside the channel with 3 obstacles within it is considered and compared with the results of Korichi and Oufer. (2005). These results are obtained for Re=400. The lattice considered is square and the channel's height is divided into 160 cells. Here, the Nusselt curve has been calculated and plotted on extended surfaces. As shown in Fig. 3, the results are in good agreement with Korichi's work.

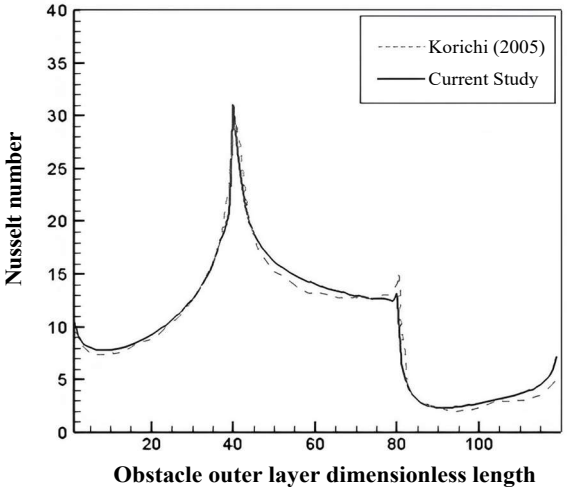

Fig. 3. Validation of the local Nusselt number distribution on obstacle Surface (Re=400).

3.2 Fluid flow and heat transfer analysis

Conjugate heat transfer, especially in complex and small sized geometries, strongly depends on the flow in the desired location. In such cases, low Re is expected because of low velocity and small dimensions of the channel. In the small sized channels where laminar flow regime exists, the viscosity leads to flow separation and circulation.

In this study, the effect of flow velocity and other parameters on heat transfer have been investigated; the intensity of heat transfer depends on the local Nu number based on the length of the obstacle. The coefficient of heat transfer between solid and fluid is equal to 1,10,100,400 W/m2K. The flow velocity is proportional to Re number, which is based on the channel height and varies between 250 and 1000. The fluid flow is in the laminar regime. The inlet fluid velocity varies from 0.3 to 5 m / s which maintains forced convective heat transfer (Anderson and Moffat, 1992).

3.2.1 Effect of Re number

The Re number is intended to be 250, 500,750 and 1000. At a low Re, flow is stable, and the velocity fluctuations decrease over a certain period of time to reach a constant velocity. In Fig. 4(a), the velocity fluctuations are plotted over time at y = 0.5 and x = 9. When Re increases, the fluid enters a transient state. When this happens, the fluctuation that occurs in the fluid decreases over time to reach a stable value. The velocity variations are shown in Fig. 4(b) for two values of Re.

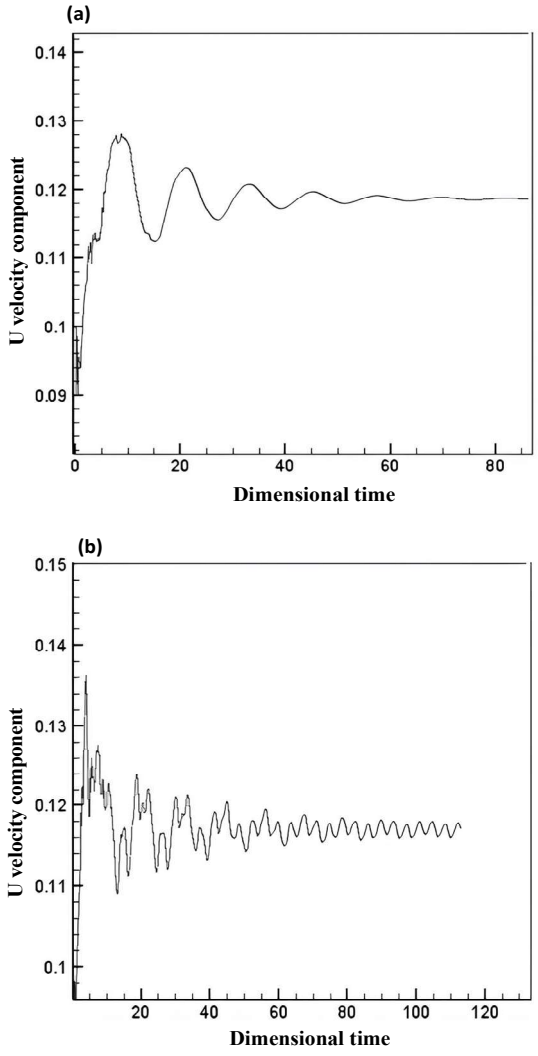

Fig. 4. Changes in the Horizontal component of velocity by time at y = 0.5 and x = 9 for a) Re = 250 and b) Re = 1000.

As fluid flows in the channel, vortices are generated behind the obstacles. At lower Reynolds number, these generated vortices remain fixed behind the obstacles. When Reynolds number exceeds a certain value, due to the increase of the cross-section (which occurs after the second obstacle) at the downstream and due to a sudden expansion, a large vortex is generated and moves forward. In this case, the flow regime changes from laminar to transient. In transient flows, these small vortices that form behind the obstacles originate, grow, and move forward in the flow direction. The order of magnitude for the velocity inside these formed vortices is 2 or 3 times less than the flow in the center of the channel. These streamlines are shown in Fig. 5. Isotherm lines are presented for various Reynolds number in Fig. 5. The dimensions of the computational domain are very large in comparison with dimensions of the obstacles. For this reason, in order to see the isothermal lines and streamlines around the obstacles, only part of the simulation domain which includes obstacles is shown in Fig. 5.

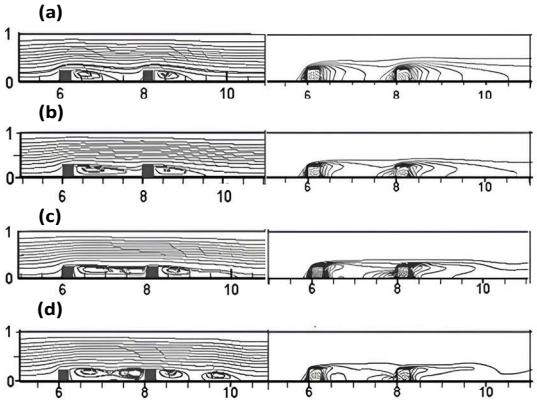

Fig. 5. Snapshot of variations of Streamlines and isothermal lines in terms of Reynolds number for k_s / k_f = 10 and Reynolds (a) 250. (b) 500 (c) 750, (d) 1000.

The heat transfer rate is characterized by the local Nusselt number based on the obstacle's outer layer dimensionless length. Time-averaged dimensionless temperature and velocity components are calculated over the simulation domain. Local and mean Nusselt numbers and dimensionless temperature are formulated as (11) and (12):

$$Nu_x = \frac{-1}{\theta_m}\frac{\partial\theta}{\partial n} \tag{11}$$

$$\theta = \frac{T - T_0}{qH/k_f} \tag{12}$$

Fig. 6 shows the variation of Nusselt number against the length of the outer surface of the obstacle for different Reynolds numbers. As seen in these figures, the Nusselt increases with increasing Re. In the lower left corner, due to the rotation of the flow and the proximity of the inlet heat flux, the Nusselt number has a relative maximal value. Near the upper left corner on the obstacle, the increases in the temperature gradient of the fluid (| ∂θf /∂n |) is due to the increase in momentum. For the obstacle left face (0.25> obstacle outer surface length> 0), and before the sudden increase of the Nusselt in the upper left corner, Nusselt has a minimum relative value. For the upper face of the obstacle (0.5> obstacle outer surface length > 0.25), the temperature gradient value is higher than the obstacle left and right face. This is due to the higher flux and, in turn, the reduction of the thickness of the boundary layer. For the obstacle right face (0.75> obstacle outer surface length > 0/5), the Nusselt increases slightly with the increase of the Reynolds number, and this increase is negligible compared to the increase in the Nusselt in the upper and left face. It is important to mention that the trend of Nusselt variation versus the length of the outer surface of the obstacle remains unchanged with Re within its range between 250 and 1000.

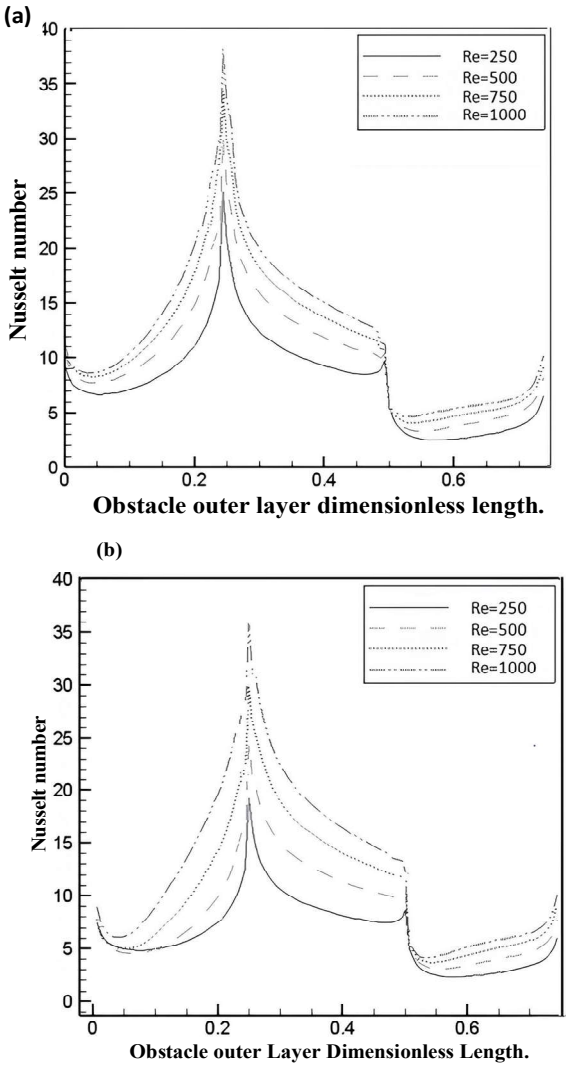

Fig. 6. Time-averaged variation of the Nusselt number in terms of the outer surface of the obstacle for k_s / k_f = 10. a) first obstacle b) second obstacle

3.2.2 Effect of conductivity ratio

One of the parameters that plays an important role in heat transfer is the conductivity ratio between the solid and the fluid

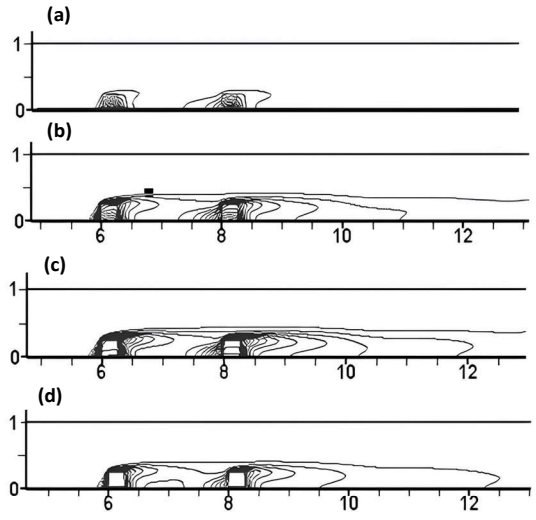

Fig 7. Variation of time-averaged isotherms for different Solid-Fluid thermal conductivity ratio for Re =600. a) $k_s / k_f = 1$ b) $k_s / k_f = 10$ c) $k_s / k_f = 100$ d) $k_s / k_f = 400$

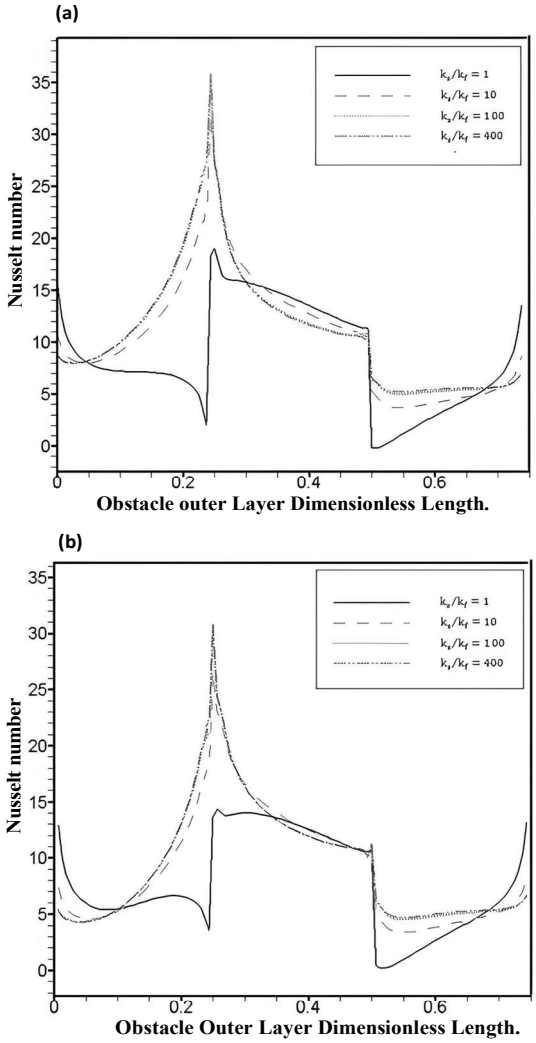

Fig. 8. Time-averaged variation of Nusselt in terms of the outer surface of the obstacle for the ratio of different Solid-Fluid thermal conductivity ratio for Re =600. a) first obstacle b) second obstacle

(k_s / k_f). By increasing the conductivity ratio, the internal resistance against thermal flux decreases, which also reduces the maximum temperature and reduces the internal temperature gradient. When the conductivity order of magnitude for solid obstacles is 2 or 3 times larger than the conductivity of fluid, the obstacle behaves as an isothermal object. Fig. 7 shows the dimensionless isothermal curves. Here, Re is fixed and equal to 600. The thermal conductivity ratio between solid and fuel (k_s / k_f) is set to 1, 10, 100, and 400. For (k_s / k_f)= 1, the density of the isothermal curves for both the solid and fluid is identical. When this ratio increases, gradually the temperature of the obstacle decreases, and the obstacle itself behaves as an isothermal object.

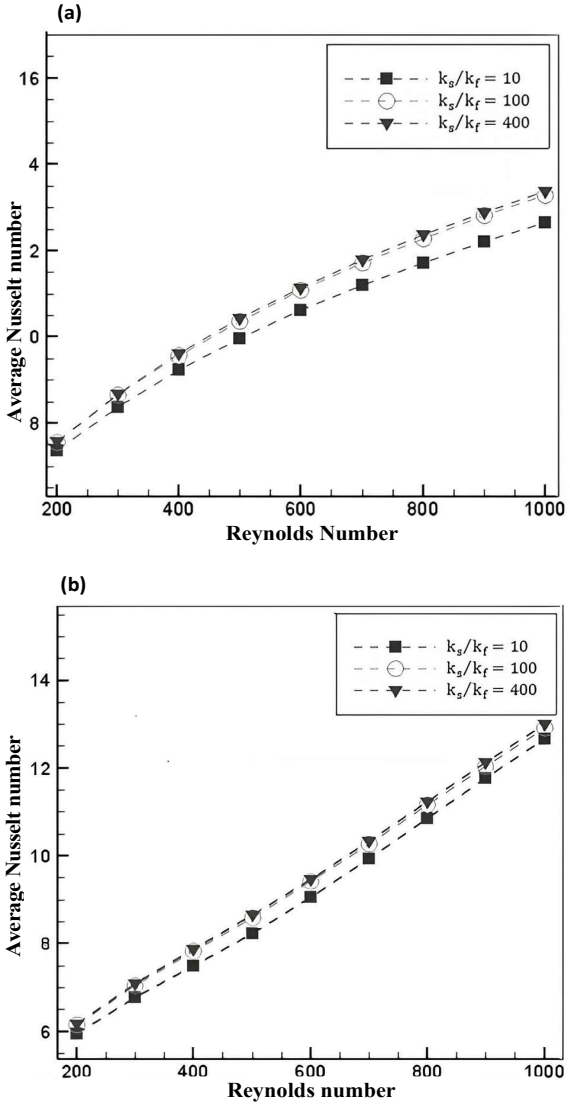

Fig. 9. Time-averaged variations of the average Nusselt number with variation of the Reynolds number for k_s /k_f=10, 100, 400. a) first obstacle b) second obstacle

Fig. 8 shows the distribution of local Nusselt on extended surfaces. When the ratio k_s / k_f = 1, the behavior of Nusselt is completely different from when this ratio is higher; and in this case, the obstacle behaves such as heat insulator. When the thermal conductivity ratio of the solid and the fluid increases,

the difference in the surface temperature of the obstacle is almost negligible. For a situation in which this ratio is greater than 100, the distribution of Nusselt does not change, and solid obstacles behave as an isothermal object.

The mean time-averaged variation of Nusselt in terms of Re for different conductivity ratios of solids and fluids is shown in Fig. 9. As Re increases, the magnitude of heat transfer from the obstacle surface increases. Also, increasing thermal conductivity ratio between solid and fluid causes reduction of the heat flux resistance in the solid obstacle.

4. CONCLUSIONS

In this paper, fluid flow and heat transfer in a two-dimensional channel with two obstacles located on its lower wall were investigated. A two-dimensional Lattice Boltzmann model was used to study the conjugate heat transfer between solid and fluid and the effect of many parameters on heat transfer was investigated. Compared to the commercial CFD methods, the use of the Lattice Boltzmann method has many advantages. One of the benefits of this is the simple application of the Boltzmann's method for complex geometries and the simple calculation process. In order to demonstrate the flexibility of this method, many parameters such as Reynolds number, thermal conductivity ratio between solid and fluid, and also distance between obstacles were investigated. The obstacle was assumed to heat up with constant heat flux, which actually simulates the heat transfer in electronic equipment. The results showed that with the increase of Reynolds number, the total heat transfer rate increases, and also the highest heat transfer occurs at the corners of the obstacles. The solid conductivity coefficient plays an important role in heat transfer. As conductivity ratio between solid and fluid increases, the resistance to heat transfer decreases and this means more heat transfer for extended surfaces.

REFERENCES

Nejadseifi, M., Kiani-Oshtorjani, M., Tynjälä, T., and Jalali, P. (2024). Permeability of partially to fully randomized arrays of square disks: A lattice Boltzmann approach. Journal of Porous Media, 27(3), 85-99.

Sara, O. N., Pekdemir, T., Yapici, S. I., and Yilmaz, M. (2001). Heat-transfer enhancement in a channel flow with perforated rectangular blocks. International Journal of Heat and Fluid Flow, 22(5), 509–518.

Suss, A., Mary, I., Le Garrec, T., and Marié, S. (2023). Comprehensive comparison between the lattice Boltzmann and Navier–Stokes methods for aerodynamic and aeroacoustic applications. Computers ans Fluids, 257, 105881.

Ataei-Dadavi, I., Rounaghi, N., Chakkingal, M., Kenjeres, S., Kleijn, C. R.,and Tummers, M. J. (2019). An experimental study of flow and heat transfer in a differentially side heated cavity filled with coarse porous media. International Journal of Heat and Mass Transfer, 143, 118591.

Bhowmik, H., and Lee, K.-S. (2009). Analysis of heat transfer and pressure drop characteristics in an offset strip fin heat exchanger. International Communications in Heat and Mass Transfer, 36(3), 259–263.

Chen, Z., Li, Q., Meier, D., and Warnecke, H.-J. (1997). Convective heat transfer and pressure loss in rectangular ducts with drop-shaped pin fins. Heat and Mass Transfer, 33, 219–224.

Chikh, S., Boumedien, A., Bouhadef, K., and Lauriat, G. (1998). Analysis of fluid flow and heat transfer in a channel with intermittent heated porous blocks. Heat and Mass Transfer, 33(5), 405–413.

Leung, C. W., Chan, T. L., Probert, S. D., and Kang, H. J. (1999). Forced convection from a horizontal ribbed rectangular base-plate penetrated by arrays of holes. Applied Energy, 62(2), 81–95.

Matsuda, V. A., Martins, I. T., Moreira, D. C., Cabezas-Gómez, L., and Bandarra Filho, E. P. (2024). A Modified Enthalpic Lattice Boltzmann Method for Simulating Conjugate Heat Transfer Problems in Non-homogeneous Media. Inventions, 9(3), 57.

Meinders, E. R., and Hanjalić, K. (2002). Experimental study of the convective heat transfer from in-line and staggered configurations of two wall-mounted cubes. International Journal of Heat and Mass Transfer, 45(3), 465–482.

Mirahsani, S., Ahmadpour, A., and Hajmohammadi, M. R. (2023). Optimal design of an array of porous obstacles in a partially heated channel using lattice Boltzmann method for the heat transfer enhancement. International Communications in Heat and Mass Transfer, 143, 106737.

Nazari, M., Kayhani, M. H., and Bagheri, A. A. H. (2013). Comparison of heat transfer in a cavity between vertical and horizontal porous layers using LBM. Modares Mechanical Engineering, 13(8), 93–107.

Paknahad, R., Siavashi, M., and Hosseini, M. (2023). Pore-scale fluid flow and conjugate heat transfer study in high porosity Voronoi metal foams using multi-relaxation-time regularized lattice Boltzmann (MRT-RLB) method. International Communications in Heat and Mass Transfer, 141, 106607.

Ramesh, K. N., Sharma, T. K., and Rao, G. A. P. (2021). Latest advancements in heat transfer enhancement in the micro-channel heat sinks: a review. Archives of Computational Methods in Engineering, 28, 3135–3165.

Anderson, A. M., and Moffat, R. J. (1992). The adiabatic heat transfer coefficient and the superposition kernel function: Part 1—Data for arrays of flatpacks for different flow conditions.

Mohammad, A. A. (2007). Applied lattice Boltzmann method for Transport phenomena, momentum, heat and mass transfer.

Korichi, A., and Oufer, L. (2005). Numerical heat transfer in a rectangular channel with mounted obstacles on upper and lower walls. International Journal of Thermal Sciences, 44(7), 644–655.

Pirouz, M. M., Farhadi, M., Sedighi, K., Nemati, H., and Fattahi, E. (2011). Lattice Boltzmann simulation of conjugate heat transfer in a rectangular channel with wall-mounted obstacles. Scientia Iranica, 18(2), 213–221.

Zou, Q., and He, X. (1997). On pressure and velocity boundary conditions for the lattice Boltzmann BGK model. Physics of Fluids, 9(6), 1591–1598.

Noble, D. R., Georgiadis, J. G., and Buckius, R. O. (1996). Comparison of accuracy and performance for lattice Boltzmann and finite difference simulations of steady viscous flow. International Journal for Numerical Methods in Fluids, 23(1), 1–18.